http://dx.doi.org/10.1016/j.jallcom.2020.154851

Microstructure and damage based constitutive modelling of hot deformation of titanium alloys

P.F. Gao [a, b], J. Guo [c], M. Zhan [a, *], F. Ma [d], Z.N. Lei [a], L. Xing [a], M.W. Fu [b, *]

[a] State Key Laboratory of Solidification Processing, Shaanxi Key Laboratory of High-Performance Precision Forming Technology and Equipment, School of Materials Science and Engineering,

Northwestern Polytechnical University, Xi'an 710072, PR China

[b] Department of Mechanical Engineering, The Hong Kong Polytechnic University, Hung Hom, Kowloon, Hong Kong, PR China

[c] Institute of chemical materials, China academy of engineering physics, Mianyang, PR China

[d] Long March Machinery Factory, China Aerospace Science and Technology Corporation, Chengdu, 610100, PR China

*Corresponding authors. E-mail address: zhanmei@nwpu.edu.cn (M. Zhan), ming.wang.fu@polyu.edu.hk (M.W. Fu)

Abstract

Developing a synthetical constitutive model describing the flow behavior, microstructure and damage evolution is necessary to achieve the accurate prediction of macroscopic deformation, microstructure and fracture during hot deformation of titanium alloy. To this end, a damage-coupled constitutive model considering microstructure evolution was developed for TA15 alloy in this work. Hot tensile tests were first conducted to analyze the microstructure, damage and flow behavior features. It was found that increasing β phase fraction and DRX fraction could supress the whole damage evolution, including void nucleation, growth and coalescence, and thus make the fracture strain increases in an exponential form. Based on experimental results, the microstructure evolution (phase transformation and DRX) was modelled using physically-based internal state variable method. The damage and fracture were modelled considering the effects of microstructure and stress state, which is realized by introducing β phase fraction, DRX fraction and stress triaxiality into the classical Gurson-Tvergaard-Needleman damage model. Then, the constitutive law considering both the microstructure and damage evolution was given. To sum up, the damage-coupled constitutive model considering microstructure evolution was established. The parameters in constitutive model were calibrated by comparing the predicted and experimental results. At last, the developed model was

successfully applied to in the finite element modelling of hot spinning of TA15 alloy tube, which can achieve the unified prediction of macroscopic deformation, microstructure, damage and fracture. The results are of great significance to the coordinated control of microstructure and damage in the hot working of titanium alloy components.

Keywords: Titanium alloy, Hot deformation, Constitutive modelling, Microstructure, Damage and fracture

1. Introduction

Titanium alloys present superior specific strength, excellent thermal stability and welding performance, which are widely used to manufacture light-weight structure components in aviation and automotive industries [1, 2]. Hot working, such as hot spinning, rolling, forging and so on, are most commonly used to process these titanium alloy components. During their hot deformation, complex hardening and softening flow behavior and significant microstructure changes may take place, which would determine the macroscopic shape evolution and final mechanical properties [3-6]. Moreover, ductile damage and fracture would also occur under severe plastic deformation, which brings about defect in the manufactured components [6-8]. Thus, elaborate processing design is necessary to avoid sensitive ductile fracture defect and obtain desired macroscopic shape and microstructure. At present, numerical simulation, as alternative for the traditional trial-and-error experiment method, has become an indispensable tool in the optimization of hot working process. It requires the simulation model to be able to predict the macroscopic deformation, microstructure evolution, as well as the ductile damage and fracture precisely at the same time. To this end, it is necessary to establish a synthetical constitutive model which can describe the flow behavior, microstructure evolution, damage and fracture criterion of titanium alloy during hot deformation.

As well known, significant microstructure changes, including phase transformation, dislocation multiplication, dynamic recovery (DRV), dynamic recrystallization (DRX) and so on, would occur in the hot working of titanium alloys [9, 10]. These microstructure evolutions would greatly affect the flow behavior, damage and fracture behavior. For example, dislocation multiplication causes strain hardening, while, DRV and DRX cause flow softening. The formation of defect-free DRX grains and α/β phase transformation would change the micro-scale heterogeneous deformation feature and then influence the damage and fracture behavior, i.e., the void nucleation, growth and coalescence. In addition, the damage evolution would further produce softening effect to the macroscopic flow

behavior. These characteristics bring great challenge to the development of synthetical constitutive model. Specifically, the damage evolution should be coupled in the constitutive model, moreover, the effects of microstructure evolution on them should also be considered.

By now, the flow behavior and damage fracture were modelled respectively in most reported works about hot deformation of titanium alloys. For the modelling of flow behavior, physically-based internal state variable (ISV) method is widely applied to develop the constitutive model considering underlying contribution of microstructure evolution. Luo et al. [11] developed an ISV model considering the evolutions of dislocation density, grain size and phase content to predict the hot deformation behavior of TC4 alloy. Fan and Yang [12] incorporated the ISV method into self-consistent constitutive model to predict the deformation behavior and microstructure evolution of two-phase titanium alloys. In their work, the solution strengthening, dislocation interaction, DRX, grain growth and their effects on the flow behavior were considered. Similarly, Gao et al. [13], Bai et al. [14], Babu and Lindgren [15] developed ISV-based unified constitutive equations for two-phase titanium alloys at elevated temperature, in which the flow softening caused by globularization of lamellar α was mainly considered. However, these works do not consider the damage evolution, which can not predict the ductile fracture defect and just be applicable to the smaller deformation stage rigorously.

As for the damage and fracture modelling for hot deformation of metals, Johnson and Cook [16] extended the traditional J-C fracture model to hot deformation by expressing the strain to fracture as a function of temperature, strain rate and pressure. He et al. [17] correlated the critical damage factor in classical Oyane fracture model with deformation temperature, strain rate and activation energy of DRX, which makes it applicable to predict the fracture during hot working of 30Cr2Ni4MoV steel. Similarly, Zhan et al. [8] also adapted the traditional Oyane fracture model to develop a thermal damage model for the hot deformation of TA15 alloy. In this work, the damage threshold was correlated with deformation temperature and strain rate by introducing the Zener-Hollomon factor. However, these works are uncoupled fracture models, which do not consider the damage induced flow softening.

Recently, some primary works about damage-coupled constitutive modelling for hot deformation of metals have been reported. Tang et al. [18] modified the classical Lemaitre damage model to take the dependency of damage on temperature and strain rate into account, which can realize the predictions of damage induced softening and fracture during hot stamping of high strength steel. Yang et al. [19] and Li et al. [20] developed a set of damage-coupled constitutive equations to model the flow behavior and

damage evolution in hot deformation of titanium alloys. In their works, the damage evolution and its softening effect to the flow behavior are characterized by a scalar damage variable. However, the effect of hot deformation on damage behavior is modelled by incorporating temperature and strain rate into the damage model parameters in the above works, so that the underlying effect mechanisms of microstructure evolution on damage and fracture behavior can not be captured. As mentioned above, there exist complex microstructure evolutions, such as dislocation evolution, DRX and α/β phase transformation in hot deformation of titanium alloy, and which greatly affects the damage and flow behavior. To reveal and predict the underlying relationship among microstructure evolution, damage evolution and flow behavior, it is still needed to develop a damage-coupled constitutive model for hot deformation of titanium alloy considering microstructure evolution.

In this paper, hot tensile tests were conducted to obtain the flow behavior and fracture feature of TA15 alloy at different conditions. Meanwhile, the microstructure evolution and its effects on damage and fracture behavior were analyzed. Based on the experimental results, a damage-coupled constitutive model considering microstructure evolution for hot deformation of TA15 alloy was established. The model is described in four aspects: microstructure modelling based on ISV method, damage modelling based on (Gurson-Tvergaard-Needleman) GTN model, constitutive law and numerical implementation. At last, the model parameters were determined and validated by applying to the simulation of hot spinning of TA15 alloy.

2. Material and experiment

The material used in this work is a wrought two-phase TA15 alloy in the form of round bar. Its chemical composition is given in Table 1. The initial microstructure of the as-received material is consisted of equiaxed primary α phase within the transformed β matrix (secondary α phase and β phase), as shown in Fig. 1. Its β-transus temperature is 1263 K.

Table 1 The chemical composition of TA15 alloy

Element	Ti	Al	Mo	Zr	V	Fe	Impurity
Content (wt.%)	Matrix	6.1-6.5	0.9-1.2	1.9-2.2	0.8-1.3	0.25	<0.3

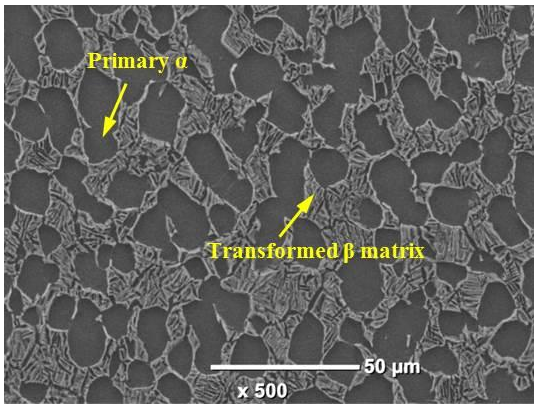

Fig. 1 Initial microstructure of the as received TA15 alloy.

Uniaxial tensile test samples were machined from the initial material, whose shape and size are shown in Fig. 2. Then, the hot tensile tests were conducted on a SANS CMT 5205 electrical test machine under isothermal condition. In the tensile test, the samples were heated to deformation temperature, held for 10 min, stretched to fracture at a constant strain rate. In this work, the uniaxial tensile tests were carried out at four temperatures (973, 1023, 1073, and 1123 K) and three strain rates (10^{-3}, 10^{-2}, and 10^{-1} s^{-1}). After tensile deformation, the samples were water quenched to maintain the microstructure characteristics at high temperature. Besides, the force-displacement curves were captured, based on which the stress-strain curves in tensile tests were also calculated.

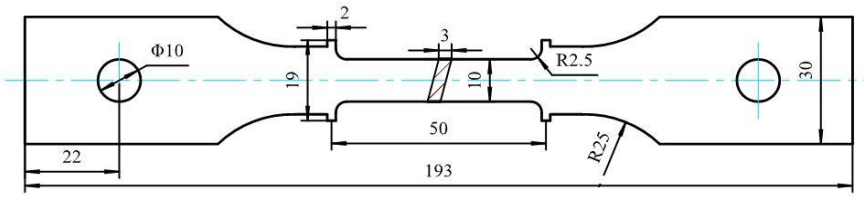

Fig. 2 Schematic of the uniaxial tensile test specimen [21]. Unit: mm.

The deformed samples were also sectioned vertical to the thickness direction and prepared for metallographic examination. The microstructure at different conditions were observed by scanning electron microscope (SEM) using standard techniques. Moreover, the microstructure was also examined by electron back-scattered diffraction (EBSD). Before EBSD, the samples were electro-polished with a solution (5% $HClO_4$ + 30% CH_3OH + 65% $C_4H_{10}O$) with a voltage of 25V. After EBSD, the microstructure characteristics were quantitatively analyzed through the HKL-Channel 5 software.

It is well known that the stress state plays great effect on the damage and fracture behavior during deformation of metals [22, 23]. And, there always exist various stress states during hot working process.

Thus, to investigate and incorporate the effect of stress state on damage and fracture feature into the constitutive model, another three types of tensile samples were also designed to achieve deformation with different stress states, as shown Fig. 3. Hot tensile testes were also conducted on these samples at different conditions. To obtain the stress states of four types samples in Fig. 2 and 4 during deformation, conventional finite element simulation was conducted. The simulation results show that the stress triaxiality at sample center are 0.33, 0.6, 0.26 and 0.1 for the uniaxial tension, notch tension, 45° shear and 0° shear tensile tests, respectively. Moreover, the local strain and fracture strain of sample were captured by simulation, which will provide basis for the microstructure analysis and constitutive modelling.

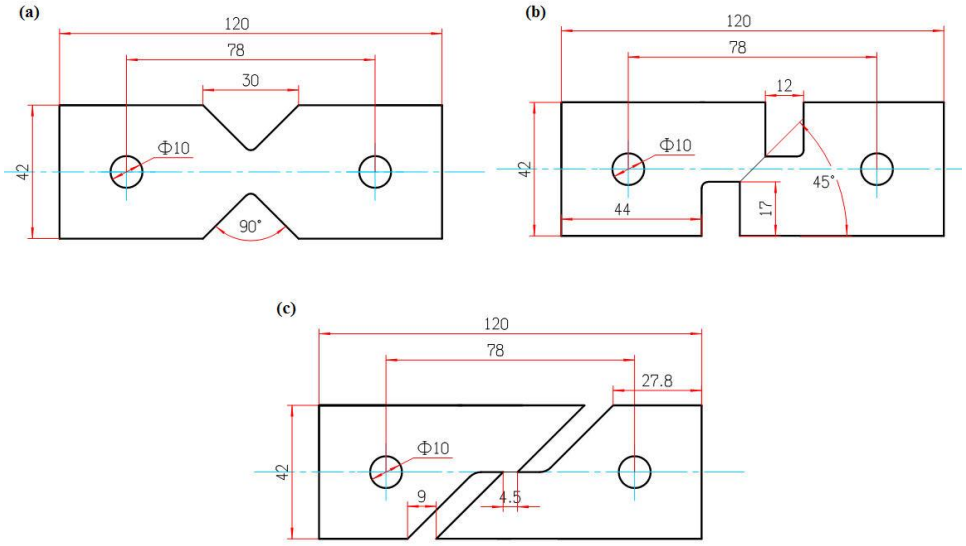

Fig. 3 Schematic of samples for tensile tests with different stress states: (a) notch tension, (b) 45° shear (c) 0° shear. Unit: mm.

3. Experiment results

In this section, the experimental flow behavior of TA15 alloy during hot deformation will be first introduced, which is the basic data for constitutive modelling. Then, the characteristics of microstructure evolution, damage and fracture, especially the effect of microstructure evolution on damage and fracture will be analyzed. These will provide important guidance for modelling the dependences of damage and flow behavior on microstructure evolution.

3.1 Flow behavior

Fig. 4 shows the stress-strain curves of uniaxial tensile tests at different conditions. It can be seen that the variation of stress with strain at any condition can be divided roughly into four stages as

follows. (1) elastic deformation stage: the stress increases linearly with strain in this stage. (2) work hardening stage: plastic deformation occurs and the flow stress increases gradually with strain in this stage, which is mainly caused by the dislocation multiplication. (3) flow softening stage: the stress decreases after peak stress in this stage. DRV and DRX are the main reasons for the softening, meanwhile, damage evolution also contributes to the softening to some extent. (4) fracture stage: the stress decreases quickly with strain and fracture occurs due to the dramatic development of damage. It can be found that the flow behavior is closely related to the microstructure and damage evolution, which should be incorporated in the constitutive modelling.

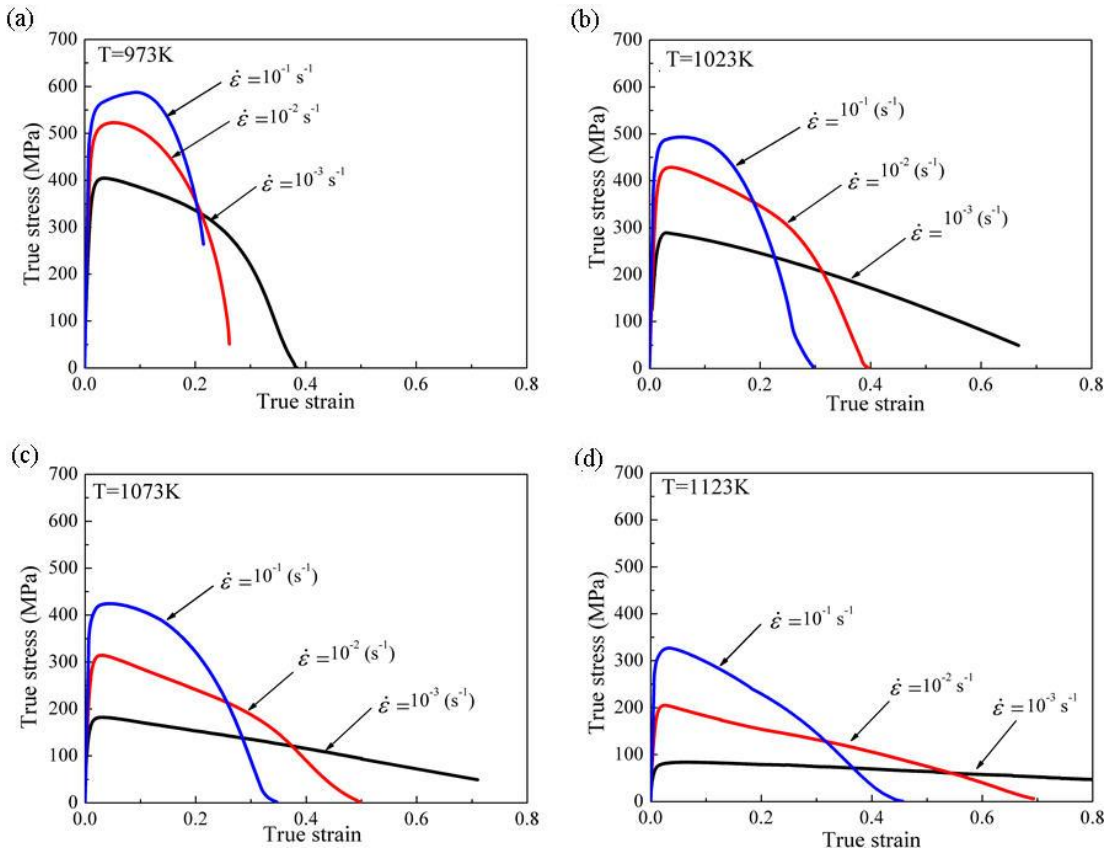

Fig. 4 Flow stress of uniaxial tensile tests with different strain rates and the temperatures.

3.2 Microstructure, damage and fracture

As a typical example, the microstructure evolution at temperature of 973 K and strain rate of 10^{-3} s^{-1} is shown in Fig. 5 [21]. At smaller strain of 0.03, few DRX grain is observed and the density of low-angle boundaries (<15°) (LAB) is relatively low (Fig. 5(c)). As the strain increases to 0.15, quantities of α DRX grains are observed around the primary coarse grain, and the density of LABs increases dramatically (Fig. 5(d)). These suggest that DRX of α phase is an important microstructure phenomenon in the hot tensile deformation of TA15 alloy. As well known, DRX is a key factor for the

flow softening, thus which must be considered in the constitutive modelling. In addition, Shang et al. [24] has proposed that DRX induced softening effect may relieve the local stress concentration and then suppress the void nucleation, growth and coalescence during hot deformation of metallic materials. Thus, the quantitative effect of DRX on damage evolution in hot deformation of TA15 alloy will be analyzed below to lay basis for the damage modelling considering microstructure evolution.

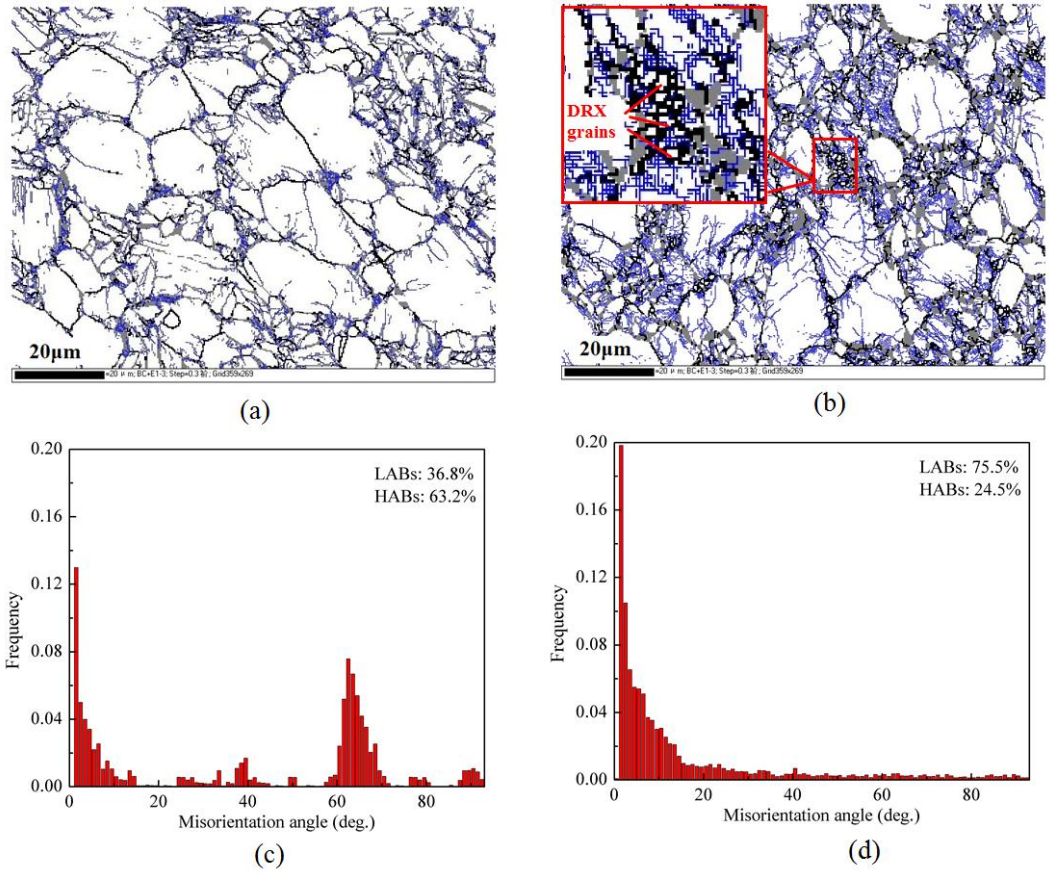

Fig. 5 Evolutions of grain-boundary and misorientation at 973 K, 10^{-3} s^{-1}: (a, c) strain of 0.03, (b, d) strain of 0.15 [21]. Blue lines indicate LABs (<15°) and black lines indicate HABs (>15°).

Previous work suggested that the phase contents and DRX kinetics are strongly dependent on temperature during hot deformation of TA15 alloy [21]. Thus, the effect of microstructure on damage behavior, including void nucleation (Fig. 6), void growth (Fig. 7) and void coalescence (Fig. 8), were analyzed by comparing the situations at different temperatures of 973, 1023 and 1073K. From Fig. 6, it can be seen that the void nucleation rate decreases with the increase of temperature, which is mainly caused by two reasons. One reason is with temperature increasing, the β phase fraction would increase and undertake more deformation due to its lower hardness than α phase. This will reduce the deformation heterogeneity between two phases, thus relieve the driving force for void nucleation.

Another reason is the DRX kinetics increases with temperature. It will cause flow softening and relieve the stress concentration, then also suppress the void nucleation. The relief of stress concentration caused by DRX would also suppress the void growth, as shown in Fig. 7. At lower DRX fraction (Fig. 7(a) and (b)), the void grows towards the direction without DRX grains. At higher DRX fraction (Fig. 7(c)), the void is surrounded by DRX grains, whose size is obviously smaller than those in Fig.7 (a) and (b). These suggest that DRX presents obstacle effect to the void growth. As for the void coalescence, it is mainly achieved by the ligament necking driven by local stress concentration. The gap between two voids to be coalesced (coalescence gap) is an important indicator evaluating the difficulty degree for the occurrence of void coalescence [25]. From Fig. 8, it can be seen that the coalescence gap decreases gradually from Fig. 8 (a) to (c). It suggests that the increase of DRX kinetic would relieve the stress concentration and then retard the void coalescence.

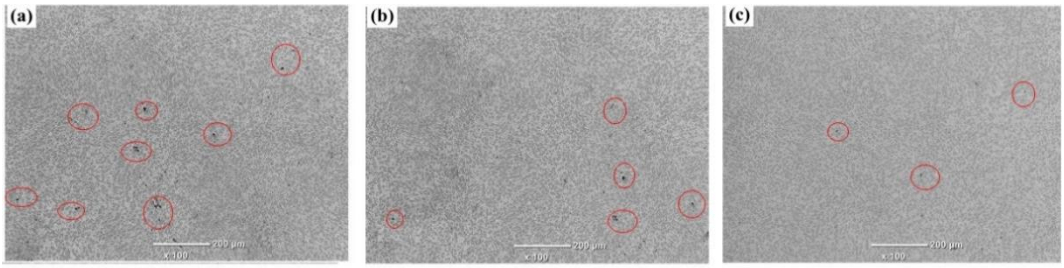

Fig. 6 Void nucleation at the strain rate of $10^{-2}s^{-1}$ and different temperatures: (a) 973K; (b) 1023K; (c) 1073K.

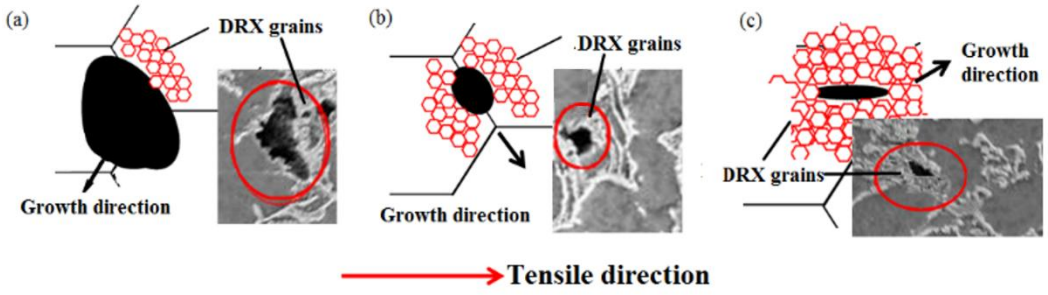

Fig. 7 Void growth at the strain rate of $10^{-2}s^{-1}$ and different temperatures: (a) 973K; (b) 1023K; (c) 1073K.

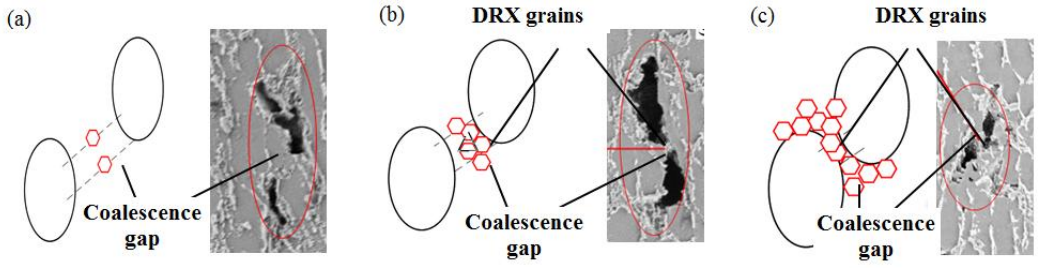

Fig. 8 Void coalescence at the strain rate of $10^{-2}s^{-1}$ and different temperatures: (a) 973K; (b) 1023K; (c) 1073K.

The above analyses indicate that increasing β phase and DRX fractions would supress the whole damage evolution, including void nucleation, growth and coalescence, which may further affect the plasticity (fracture strain) of material. Fig. 9 shows the variation of fracture strain with β phase and DRX fraction at different conditions. It can be seen that the fracture strain increases with both of β phase fraction and DRX fraction in an exponential form.

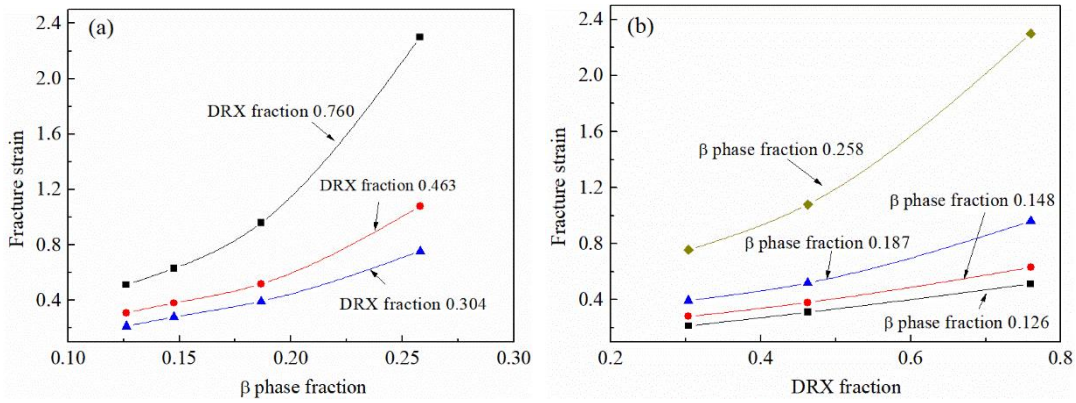

Fig. 9 Variation of fracture strain with β phase fraction (a) and DRX fraction (b) at different conditions.

As mentioned above, besides microstructure evolution, the stress state will also affect the damage and fracture. Fig. 10 shows the variation of fracture strain with stress state from tensile experiments at 1023K. It can be seen that the fracture strain first increases and then decreases with stress triaxiality. The maximum fracture strain is achieved at the stress triaxiality of 0.33 corresponding to the uniaxial tensile test. While, the minimum fracture strain is achieved at the stress triaxiality of 0.6 corresponding to the notch tensile test. The above variation laws of fracture strain with microstructure and stress triaxiality lay important foundations for integrating the microstructure and stress state effects into damage modelling, which will be described in Section 4.2.

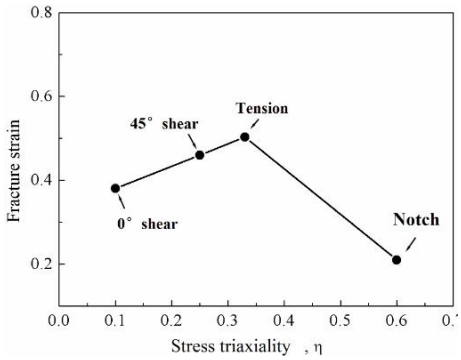

Fig. 10 Variation of fracture strain with stress triaxiality at 1023K.

4. Establishment of constitutive model

In this section, the damage-coupled constitutive model considering microstructure evolution will be developed based on the above experimental results. Fig. 11 shows the train of thought for constitutive modelling, which mainly consists of three parts: microstructure modelling, damage modelling and constitutive law. For microstructure modelling, an ISV based model considering the variation of phase fraction, dislocation multiplication, DRV, DRX and loss of Hall-Petch strengthening was applied. The damage model was derived on basis of classical void-based GTN model. It considers the effects of microstructure and stress state on damage evolution (including void nucleation, growth and coalescence) by introducing β phase fraction, DRX fraction and stress triaxiality into the GTN model. At last, the constitutive law was developed based on the microstructure and damage models. The flow stress only considering microstructure evolution was first calculated as the matrix stress of material. On this basis, the final equivalent stress considering damage evolution would be obtained. As a result, the damage-coupled constitutive model considering microstructure evolution was achieved, which could realize the unified predictions of flow stress, microstructure, damage and fracture during hot deformation of titanium alloy.

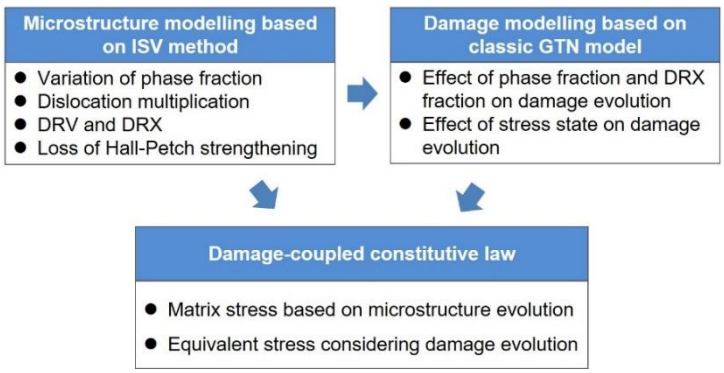

Fig. 11 Train of thought for damage-coupled constitutive modelling considering microstructure evolution.

4.1 Microstructure modelling

An ISV based microstructure model considering the variation of phase fraction, dislocation density variation, DRX and loss of Hall-Petch strengthening was applied to describe the microstructure evolution in hot deformation of titanium alloy. It was developed by the authors in previous work [21], which will be briefly described as follows. The α phase fraction (f_α) and β phase fraction (f_β) can be calculated by the following equations, respectively.

$$\begin{cases} f_\alpha = \zeta_1 \left\{ 1 - \exp\left[\zeta_2 \left(\zeta_3 - T \right) \right] \right\} \\ f_\beta = 1 - f_\alpha \end{cases} \tag{1}$$

where T is temperature. ζ_1, ζ_2 and ζ_3 are material constants with the values of 0.9, -0.012 and 1263K, respectively, for TA15 alloy [21].

The variation of dislocation density is represented by KM model (eq. (2)) [26], which considers the working hardening and DRV.

$$\frac{\mathrm{d}\rho}{\mathrm{d}\bar{\varepsilon}_m^p} = k_1 \sqrt{\rho} - k_2 \rho \tag{2}$$

where ρ is dislocation density, $\bar{\varepsilon}_m^p$ is the plastic strain of matrix, k_1 describes the athermal dislocation storage. k_2 evaluates the thermally activated dynamic recovery through dislocation cross-slip or climb, which is related to deformation temperature and strain rate:

$$k_2 = k_{20} \left[\dot{\bar{\varepsilon}}_m^p \exp\left(Q_{act} / RT \right) \right]^{-1/n} \tag{3}$$

where Q_{act} is the activation energy, R is the gas constant (8.314J/(mol·K)), k_{20} and n are material constants.

For the important microstructure phenomenon DRX, its fraction evolution during hot deformation can be expressed by:

$$\dot{S} = c_0 \left(1 - S \right) \left(\dot{\bar{\varepsilon}}_m^p \right)^{c_1} \theta \left(\varepsilon_p - \varepsilon_c \right) M_b \, P / d \tag{4}$$

where S is the DRX fraction, θ is step function, c_0 and c_1 are material constants, ε_c, M_b, P and d are the critical strain for occurrence of DRX, grain-boundary mobility, driving force per unit area and average grain diameter, respectively. Their detailed forms will be described as follows. The critical strain ε_c is a function of temperature and strain rate:

$$\varepsilon_c = \varphi_0 \left(\dot{\bar{\varepsilon}}_m^p\right)^{\varphi_1} \left[\exp\left(\frac{Q_{act}}{RT}\right)\right]^{\varphi_2} \tag{5}$$

where φ_0, φ_1, and φ_2 are material constants. The grain-boundary mobility M_b in eq. (4) can be expressed by

$$M_b = \frac{\delta D_0 b}{kT} \exp\left(-\frac{Q_{pd}}{RT}\right) \tag{6}$$

where δ is characteristic grain-boundary thickness, D_0 is self-diffusion constant, k is Boltzmann's constant, and Q_{pd} is boundary-diffusion activation energy. The driving force per unit area P takes the form:

$$P = \rho G b^2 \tag{7}$$

where Gb^2 is the linear energy of the dislocation. Considering the static growth and DRX-induced grain refinement, the evolution of average grain diameter can be expressed as:

$$\dot{d} = \alpha_1 d^{-\gamma_1} - \alpha_2 \dot{S}^{\gamma_2} d^{\gamma_3} \tag{8}$$

where d is average grain size, α_1, α_2, γ_1, γ_2, and γ_3 are material constants.

It should be noted that DRX will also cause dislocation annihilation, which should also be considered in the variation of dislocation density. Thus, the evolution of density can be expressed in the form:

$$\dot{\rho} = \dot{\bar{\varepsilon}}_m^p \left(k_1 \sqrt{\rho} - k_2 \rho\right) - \rho \dot{S} / \left(1 - S\right) \tag{9}$$

Semiatin and Bieler [27] have reported that the loss of grain-boundary (α/β interface) strengthening, i.e., Hall-Petch strengthening, is also a critical microstructure phenomenon and plays great role in the flow softening. Thus, the loss of Hall-Petch strengthening has also been considered in the microstructure modelling. The Hall-Petch effect was evaluated by

$$K_{HP} = HG\sqrt{b} \tag{10}$$

where K_{HP} is Hall-Petch coefficient, H takes the form of

$$H = \lambda H_0 \tag{11}$$

where λ is a coefficient with an initial value of 1 and varies with strain according to the following equation:

$$\mathrm{d}\lambda / \mathrm{d}\bar{\varepsilon}_m^p = c_\lambda \left(\lambda_{ss} - \lambda\right) \tag{12}$$

where c_λ and λ_{ss} are material constants. H_0 in eq. (11) is a function of temperature, strain rate, and phase volume fraction:

$$H_0 = H_{ref}\left(\dot{\bar{\varepsilon}}_m^p\right)^{\psi_1}\left(\exp\left(\frac{Q_{act}}{RT}\right)\right)^{\psi_2}\left(\exp\left(f_\alpha\right)\right)^{\psi_3} \tag{13}$$

where H_{ref}, ψ_1, ψ_2, and ψ_3 are material constants.

4.2 Damage modelling

As well known, the GTN model developed by Gurson, Tvergaard and Needleman [28-30] is a well-accepted damage-mechanism-based model to predict the damage and fracture of ductile metals. It is very suitable to describe the ductile fracture through void nucleation, growth and coalescence, thus which is applied in this work. The GTN model is formulated as:

$$\Phi = (\frac{\bar{\sigma}}{\sigma_m})^2 + 2q_1 f^* \cosh(-\frac{3}{2}\frac{q_2\sigma_H}{\sigma_m}) - (1+q_1{}^2 f^{*2}) = 0 \tag{14}$$

where Φ is the yield surface of material. $\bar{\sigma}$, σ_m, and σ_H are the von Mises equivalent stress, flow stress of the undamaged matrix material and hydrostatic stress, respectively. q_1 and q_2 are fitting coefficients. Tvergaard [30, 31] has proposed that taking q_1 as 1.5 and q_2 as 1 can promote the predictive ability for the material with lower hardening exponent. Since titanium alloy is right a material with lower hardening exponent, thus they are used in this study. f^* is equivalent void volume fraction evaluating the damage degree, which is a function of void volume fraction f:

$$f^* = \begin{cases} f & f \le f_c \\ f_c + \kappa(f - f_c) & f > f_c \end{cases} \tag{15}$$

where, κ is accelerating factor for void growth and represented by

$$\kappa = (f_u - f_c)/(f_f - f_c) \tag{16}$$

where f_u=1 / q_1, which is the critical void volume fraction when the stress-carrying capacity vanishes, f_c and f_f are the critical void volume fraction for occurrence of void coalescence, and the critical void volume fraction for fracture.

The description of void volume fraction variation, i.e., damage evolution, is the key part in GTN model. It is derived from the void nucleation, void growth and shear effect as the following equation:

$$\mathrm{d}f = \mathrm{d}f_g + \mathrm{d}f_n + \mathrm{d}f_s \tag{17}$$

where the first term $\mathrm{d}f_g$ evaluates the void growth and is related to the plastic volumetric strain:

$$\mathrm{d}f_g = (1-f)\mathrm{d}\varepsilon_{kk}^p \tag{18}$$

where $\mathrm{d}\varepsilon_{kk}^p$ is the plastic volumetric strain increment induced by hydrostatic stress. The second term in eq. (17) $\mathrm{d}f_n$ represents the void nucleation and is expressed by the formulation proposed by Chu and Needleman [32]:

$$\mathrm{d}f_n = A\mathrm{d}\bar{\varepsilon}_m^p \tag{19}$$

where $A = \frac{f_N}{s_N\sqrt{2\pi}}\exp\left(-\frac{1}{2}\left(\frac{\bar{\varepsilon}_m^p - \varepsilon_N}{s_N}\right)\right)$, $\mathrm{d}\bar{\varepsilon}_m^p$ is equivalent plastic strain increment of matrix, f_N is volume fraction of nucleated voids, ε_N is nucleation strain, s_N is standard deviation of nucleation strain. The third term in eq. (17) $\mathrm{d}f_s$ estimates the contribution of shear effect to the variation of void volume fraction, through which the effect of stress state on damage evolution can be considered. The NH model proposed by Nahshon and Hutchinson [22] is used here to represent this effect:

$$\mathrm{d}f_s = k_w w f \frac{s_{ij}\mathrm{d}\varepsilon_{ij}^p}{\bar{\sigma}} \tag{20}$$

where k_w is the magnitude of damage growth rate in pure shear state, s_{ij} is deviatoric stress tensor, $\mathrm{d}\varepsilon_{ij}^p$ is plastic strain increment, w is a function describing the stress state:

$$w = 1 - \left(\frac{27J_3}{2\bar{\sigma}^3}\right)^2 \tag{21}$$

where J_3 is the third invariant of deviator stress. w locates in the range between 0 and 1. At compression and tensile state, w equals 0. At pure shear stress state, w equals 1.

As mentioned in Section 3.2, β phase and DRX fractions both have great effects on the void nucleation, growth and coalescence in the hot deformation of TA15 alloy. However, the classical equations describing void evolution (eq. (15-19)) does not consider the effects of microstructure evolution. To overcome this problem, they are improved by introducing β phase fraction and DRX fraction in an exponential form according to the exponential variation law of fracture strain in Fig. 9. The detail improvements for equations describing damage evolution are as follows. Nucleation strain

ε_N is the critical factor determining development of void nucleation, which is updated by incorporating β phase and DRX fractions:

$$\varepsilon_N = \varepsilon_{N_0}\left[\exp\left(C_s S + C_\beta f_\beta^*\right)\right] \tag{22}$$

For void growth, a growth factor χ depending on β phase and DRX fractions is introduced in eq. (18) to consider the microstructure effect. The updated formulation for void growth rate is:

$$\mathrm{d}f_g = \chi\left(1-f\right)\mathrm{d}\varepsilon_{kk}^p = \chi_0\left[\exp\left(D_s S + D_\beta f_\beta^*\right)\right]\left(1-f\right)\mathrm{d}\varepsilon_{kk}^p \tag{23}$$

Similarly, the critical void volume fraction for void coalescence f_c is also improved to consider the effects of β phase and DRX fractions:

$$f_c = f_{c_0}\left[\exp\left(E_s S + E_\beta f_\beta^*\right)\right] \tag{24}$$

In eq. (22-24), ε_{N_0}, χ_0, f_{c_0} are reference values of nucleation strain, growth factor and critical void volume fraction for coalescence, respectively. χ_0 is taken as 1 in this work. While, ε_{N_0} and f_{c_0} will be determined in Section 5.1. f_β^* is a parameter related to β phase fraction, which is expressed by

$$f_\beta^* = \frac{f_\beta - f_\beta^r}{1 - f_\beta^r} \tag{25}$$

where f_β^r is reference value of β phase fraction. According to eq. (1), the β phase fraction varies little below 973K, while varies greatly above 973K. Thus, the β phase fraction at 973K is taken as the reference value. Besides, $C_\beta, D_\beta, E_\beta$ and C_s, D_s, E_s are β phase fraction and DRX fraction related coefficients.

Substituting the improved equations (22-24) into classical GTN model, the effects of microstructure (β phase and DRX fractions) on void nucleation, growth and coalescence can be considered in damage modelling.

4.3 Constitutive law

In this section, the constitutive law considering microstructure and damage evolution will be developed. First, the matrix stress only considering microstructure evolution for a polycrystal metal can be represented by [21]:

$$\sigma_m = M\tau \tag{26}$$

where M is the Taylor factor with the value of 3.06. According to the Taylor assumption, τ is the shear stress consisted of two parts, as shown below:

$$\tau = \tau^* + \tau_\mu \tag{27}$$

where τ^* is the thermally activated stress for moving dislocations through lattice and pass short-range obstacles. τ_μ is the athermal stress caused by long-range effects (such as the grain boundaries and dislocation forests). The former thermally activated stress depends on the temperature and strain rate, which can be calculated by

$$\tau^* = \tau^0 \left[1 - \left(\frac{RT}{\Delta G} \ln \frac{\dot{\varepsilon}_{ref}}{\dot{\varepsilon}_m^p} \right)^{1/q} \right]^{1/p} \tag{28}$$

where τ^0 is the mechanical threshold stress, ΔG is the activation energy for deformation, $\dot{\varepsilon}_{ref}$ is the reference strain rate. p and q are material constants. The later athermal stress mainly considers the strain-hardening and grain-boundary effects, which can be expressed by

$$\tau_\mu = \alpha G b \sqrt{\rho} + K_{HP} d^{-1/2} \tag{29}$$

where G is the shear modulus. For TA15 alloy, it is a function of temperature [10]:

$$G = 49.02 - \frac{5.821}{\exp(181/T) - 1} \tag{30}$$

α is material constant, and b is the magnitude of Burgers vector (2.95×10^{-10} m). K_{HP} and d are the Hall-Petch coefficient and average grain size, respectively, which have been described in microstructure modelling.

Combining eq. (26-30) and microstructure model in Section 4.1, the flow stress of TA15 alloy considering microstructure evolution can be calculated. It should be noted that this is the matrix stress of material without any damage, which is just applicable to predict the flow stress of titanium alloy in early deformation stage, as described in [11-15, 21]. It is still needed to substitute the matrix stress in eq. (26) into eq. (14) and calculate the equivalent stress considering damage-induced softening based on damage model in Section 4.3. This equivalent stress is right the desirable combined result considering both the microstructure and damage evolution.

4.4 Numerical implementation of the model

The proposed damage-coupled constitutive model cannot be solved analytically. The return mapping algorithm combined with implicit Euler backward method was used to realize the numerical calculation, which will be described in this section. The detailed numerical calculation procedure is given in Fig. 12.

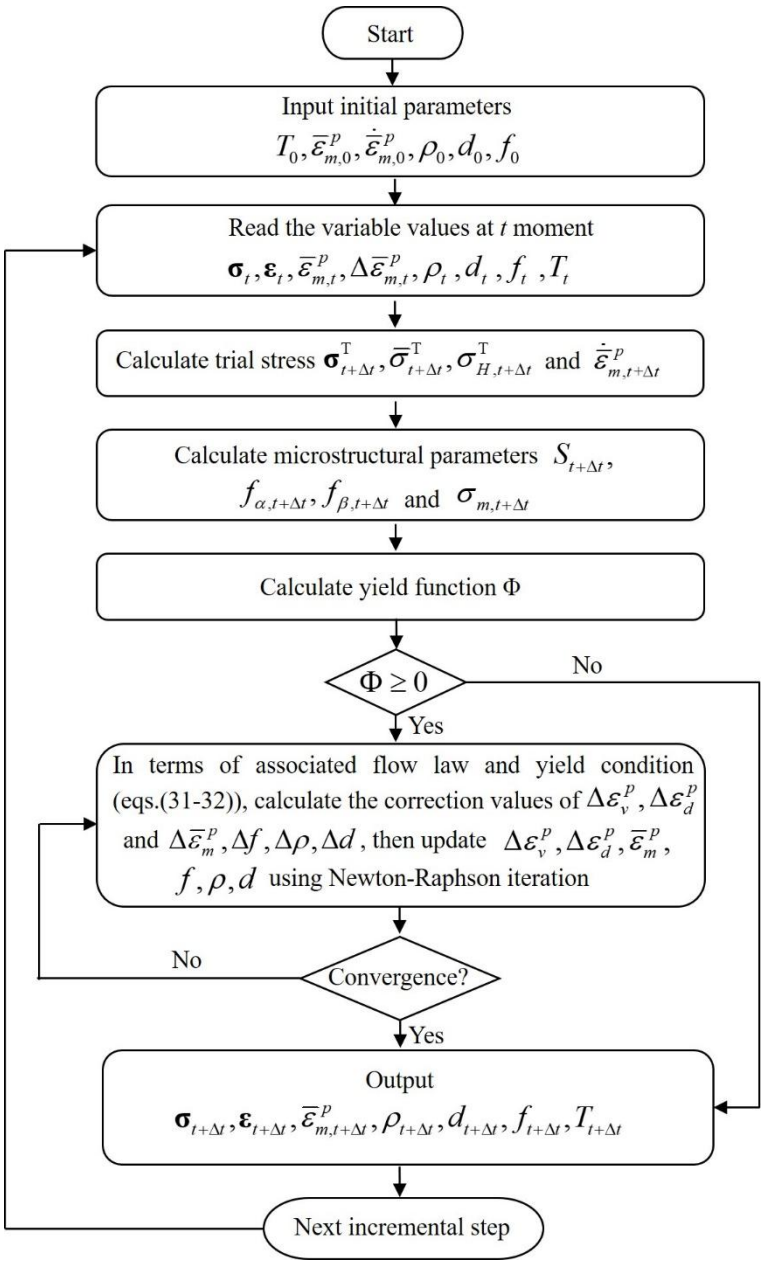

Fig. 12 Numerical calculation procedure of the damage-coupled constitutive model.

Step 1: Initialize the processing parameters ($T,\dot{\bar{\varepsilon}}_m^p$), microstructural parameters (ρ,d), equivalent plastic strain of matrix ($\bar{\varepsilon}_m^p$), volume fraction of void (f), stress tensor and strain tensor at t=0 time.

Step 2: Read the variable values of $\boldsymbol{\sigma}_t$, $\boldsymbol{\varepsilon}_t$, $\bar{\varepsilon}_{m,t}^p$, $\Delta\bar{\varepsilon}_{m,t}^p$, ρ_t , d_t , f_t and T_t at t moment.

Step 3: Calculate elastic trial stress $\boldsymbol{\sigma}_{t+\Delta t}^{\mathrm{T}}$, $\bar{\sigma}_{t+\Delta t}^{\mathrm{T}}$, $\sigma_{H,t+\Delta t}^{\mathrm{T}}$ and $\dot{\bar{\varepsilon}}_{m,t+\Delta t}^p$ at t+Δt moment.

Step 4: Calculate the microstructural parameters $S_{t+\Delta t}$, $f_{\alpha,t+\Delta t}$ and $f_{\beta,t+\Delta t}$ according to equations in Section 4.1 and $\sigma_{m,t+\Delta t}$ according to equations in Section 4.3.

Step 5: Calculate yield function：

$$F_2=\Phi\left(\bar{\sigma}_{t+\Delta t}^{\mathrm{T}},\sigma_{m,t+\Delta t},\sigma_{H,t+\Delta t}^{\mathrm{T}},\bar{\varepsilon}_{m,t}^p,f_t^*\right)$$

If F_2 < 0, the current state is pure elastic state, and $\boldsymbol{\sigma}_{t+\Delta t}=\boldsymbol{\sigma}_{t+\Delta t}^{\mathrm{T}}$. Then, go back to Step 2 and start the next incremental step.

If $F_2 \geq 0$, the current state is elastic-plastic state. Go to Step 6 and start the plastic correction.

Step 6: In terms of the associated flow law and yield condition, the following two equations are given.

$$F_1=\Delta\varepsilon_v^p\frac{\partial\Phi}{\partial\bar{\sigma}}+\Delta\varepsilon_d^p\frac{\partial\Phi}{\partial\sigma_H}=0 \tag{31}$$

$$F_2=\Phi\left(\bar{\sigma},\sigma_m,\sigma_H,\bar{\varepsilon}_m^p,f^*\right)=0 \tag{32}$$

where $\Delta\varepsilon_v^p$ and $\Delta\varepsilon_d^p$ are plastic strain increment induced by hydrostatic stress and equivalent stress, respectively. Their correction values can be obtained through solving eq. (31-32) using Newton-Raphson iteration. Then the $\Delta\varepsilon_v^p$ and $\Delta\varepsilon_d^p$ are updated.

Step 7: Calculate the increment values of $\bar{\varepsilon}_m^p$ and f according to the following equations at the current iteration. Then, the $\bar{\varepsilon}_m^p$ and f are updated.

$$\Delta\bar{\varepsilon}_m^p=\frac{-\sigma_H\Delta\varepsilon_v^p+\bar{\sigma}\Delta\varepsilon_d^p}{(1-f)\sigma_m} \tag{33}$$

$$\Delta f = \Delta f_g + \Delta f_n + \Delta f_s \tag{34}$$

Step 8: Calculate the increment values of ρ and d according to equations in Section 4.1 and update them.

Step 9: Check the yield condition and convergence condition, i.e., eq. (31-32). If $|F_1| < 10^{-10}$ and $|F_2| < 10^{-10}$, the iteration converges. Output the stress, strain and internal state variables with the values derived from the last iteration and start the next incremental step. Otherwise, go back to Step 6 and start a new iteration.

5. Model validation

5.1 Determination of model parameters

As mentioned in Section 4, the numerical calculation of constitutive model includes two main steps: (1) calculating the matrix flow stress based on microstructure model and constitutive law, (2) calculating the final equivalent flow stress based on matrix stress and damage model. Correspondingly, the model parameters were also determined in two parts: parameters in microstructure and constitutive models, and parameters in damage model.

The first part of parameters involved in microstructure and constitutive models (Section 4.1 and 4.3) were determined by genetic algorithm objective optimization method. The results of uniaxial tensile experiments at temperatures of 973, 1023, 1073, 1123 K and strain rates of 10^{-3}, 10^{-2}, 10^{-1} s^{-1} were used to calibrate the parameters. The objective functions were defined as the square of difference between experimental and numerical calculated data for stress, DRX fraction and grain size. The model parameters were determined by minimizing the sum of above objective functions. It should be noted that the later-stage stress-strain curve presenting significant flow softening cannot be used here, because which is closely related to the damage development. The detailed determination process for parameters in microstructure and constitutive law can be found in the authors' previous work [21]. The determined parameters are given in Table 2, which have been verified by the comparisons between predicted and experimental results of stress, DRX fraction and grain size.

Table 2 Determined model parameters in the microstructure and constitutive law [21]

Parameters	τ_0	ΔG	q	p	α	k_1	k_{20}
Value	352.2	419.2	0.083	0.424	0.500	4.0×10^{9}	1.2×10^{7}
Parameters	Q_{act}	n	c_0	c_1	φ_0	φ_1	φ_2
Value	602.1	6.0	1.510	0.453	5.85×10^{-5}	0.102	0.093
Parameters	δD_o	Q_b	α_1	γ_1	α_2	γ_2	γ_3
Value	0.550	295.0	1.1×10^{-7}	3.9×10^{-6}	0.026	0.9	3.9×10^{-6}
Parameters	$c_{\lambda\lambda}$	λ_{ss}	ψ_1	ψ_2	ψ_3	H_{ref}	
Value	0.8	0.05	0.105	0.497	5.004	0.0217	

On basis of determined parameters in Table 2, the established damage-coupled constitutive model was integrated into ABAQUS/Explicit via user subroutine to simulate the hot tensile tests. The simulated load-displacement results were compared with the experimental ones to calibrate the parameters in damage model (Section 4.2). The parameters in damaged model can be classified into three groups: the parameters in classical GTN model ($f_0, f_N, f_c, f_f, \varepsilon_{N_0}, S_{N_0}$) , the new introduced parameters related to microstructure features ($C_\beta, C_s, D_\beta, D_s, E_\beta, E_s$) and the parameters related to stress state (k_w). They will be calibrated in sequence below.

The parameters in classical GTN model ($f_0, f_N, f_c, f_f, \varepsilon_{N_0}, S_{N_0}$) are not relevant to the microstructure evolution, thus they are first calibrated by the uniaxial tensile test at room temperature. The parameter calibration was conducted by a careful trial-and-error method to make the simulated load-displacement curve closely match the experimental one. Table 3 lists the determined parameters in classical GTN model. From Fig. 13, it can be seen that the simulated load-displacement curves and fracture point (marked with star) agree very well with the experimental results.

Table 3 Determined parameters in the classical GTN damage model

Parameters	f_0	f_N	ε_{N_0}	S_{N_0}	f_{c_0}	f_f
Values	0.0015	0.03	0.25	0.1	0.08	0.15

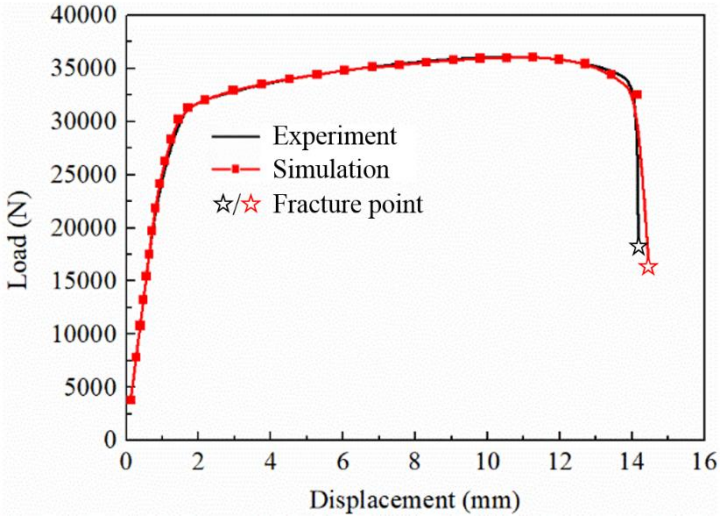

Fig. 13 Comparison between the simulated and experimental load-displacement curves of uniaxial tensile test at room temperature.

For the new introduced parameters related to microstructure features ($C_\beta, C_s, D_\beta, D_s, E_\beta, E_s$), they are calibrated in two sub-groups. The DRX related parameters C_s, D_s, E_S were first determined through the uniaxial tensile tests with various DRX kinetics. The detailed deformation conditions of tensile tests are 973K and $10^{-3}s^{-1}$, 10^{-2} s^{-1}. At these conditions, the β phase fraction is very small and changes little, thus the β phase fraction related parameters $C_\beta, D_\beta, E_\beta$ make little sense to the calculation results. The determined C_s, D_s, E_S are 1.75, -0.375 and 0.625, respectively. Using these parameters, good agreement between the simulated and experimental load-displacement curves can be obtained, as shown in Fig. 14. Then, the β phase fraction related parameters $C_\beta, D_\beta, E_\beta$ are determined by the uniaxial tensile tests with strain rate of 10^{-2} s^{-1} and temperatures of 1023K and 1123K. These samples present different β phase fraction and DRX kinetics during deformation. The determined $C_\beta, D_\beta, E_\beta$ are 0.25, -0.125, and 0.125, respectively. Fig. 15 shows the simulated results under these parameters, which are very close to the experimental results. Based on the above analysis, the determined new introduced parameters related to microstructure features in damage model are summarized in Table 4.

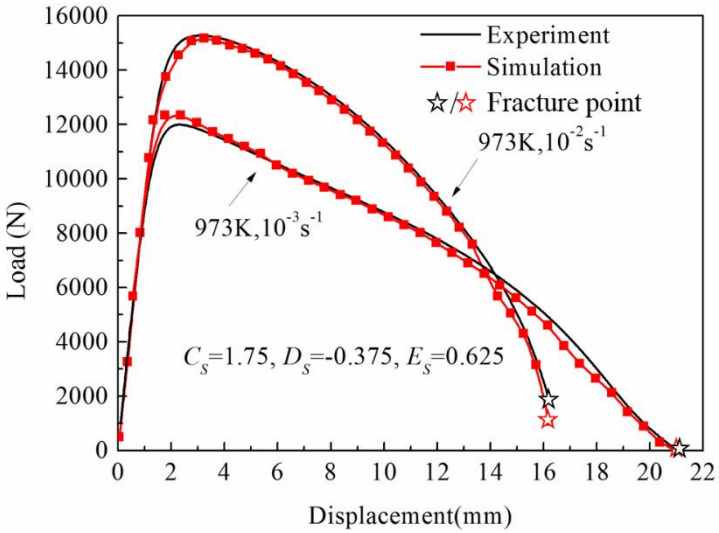

Fig. 14 Comparisons between the simulated and experimental load-displacement of the hot uniaxial tensile tests at 973K and $10^{-3}s^{-1}$, $10^{-2}s^{-1}$.

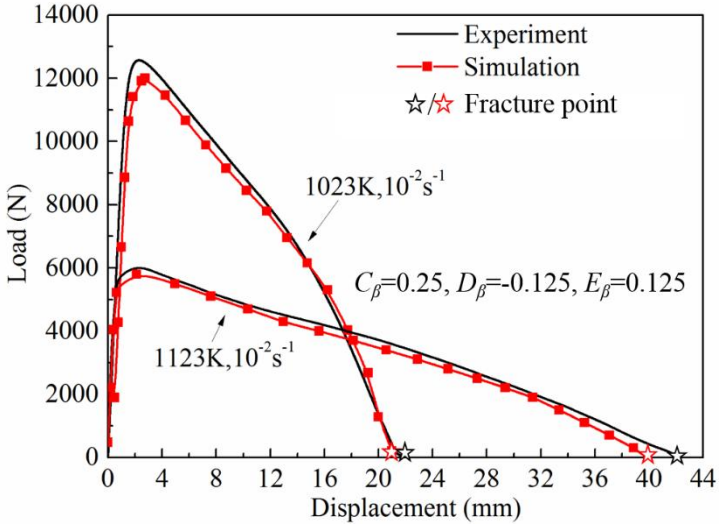

Fig. 15 Comparisons between the simulated and experimental load-displacement of the hot uniaxial tensile tests at 1023K, 1123K and $10^{-2}s^{-1}$.

Table 4 Determined new introduced parameters related to microstructure features in damage model.

Parameters	C_S	C_β	D_S	D_β	E_S	D_β
Value	1.75	0.25	-0.375	-0.125	0.625	0.125

At last, the stress state related parameter k_w was determined by tensile tests with various stress states and deformation parameters. The detailed tensile tests include 0° shear tensile test at room temperature, 45° shear tensile test at 1023K and notch tensile test at 1073K. The calibration indicates that k_w should be 1.5 to obtain well simulated load-displacement curves close to the experimental curves, as shown in Fig. 16.

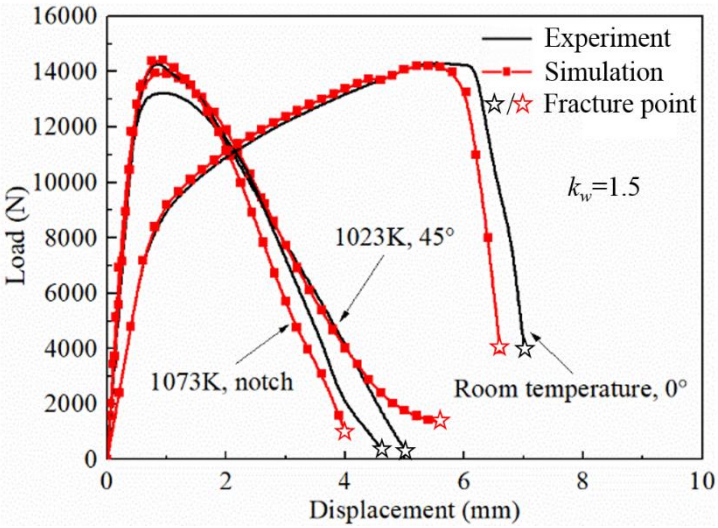

Fig. 16 Comparisons between the simulated and experimental load-displacement of tensile tests with different stress states and temperatures.

5.2 Model application

In this section, the proposed damage-coupled constitutive model was applied in a hot spinning process of TA15 alloy tube to verify its reliability. During hot spinning, the material deforms under complex temperature, strain rate and stress states, which will cause phase transformation, DRX, damage and fracture. This makes it very suitable to valid the proposed constitutive model in this study.

The FE model for hot spinning of TA15 alloy tube considering the thermal and deformation events was established, as shown in Fig. 17. The tie constraint is employed at the bottom of blank and mandrel to limit the movement of tube blank. Three rollers counterclockwise revolve and feed along the axial direction at the same time. The mandrel and roller are assumed to be isothermal analytical rigid bodies. The tube blank is set as a deformable body and discretized through C3D8RT element. To avoid mesh distortion, the ALE adaptive grid technique was applied. The proposed damage-coupled constitutive model was integrated into ABAQUS via user subroutine to describe the material behavior of tube. It should be noted that the damage just accumulates when the stress triaxiality is larger than 0. The friction between tube blank and tools was described by Coulomb's friction model with the coefficient of 0.1. For the thermal events, 90% deformation energy was set to be converted into thermal energy. The heat conduction, heat film and heat radiation were also considered to simulate the temperature change of blank. Table 5 shows the processing parameters in hot spinning.

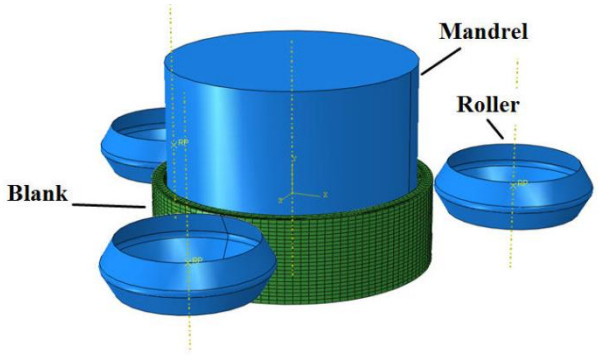

Fig. 17 FE model of hot spinning of TA15 alloy tube.

Table 5 Processing parameters of spinning

Parameters	Value
Outer diameter/inner diameter/height of tube billet (mm)	346/308/120
Mandrel diameter/height(mm)	307.5/330
Roller diameter/(mm)	116
Roller radius(mm)	10
Attack angle/°	22.5
Mandrel revolution speed(rad/s)	9.32
Roller feed rate(mm/r)	1
Spinning thinning ratio	50%
Initial spinning mandrel temperature (K)	623
Initial spinning temperature (K)	1073

To validate the FE model, hot spinning experiment was conducted at the same conditions shown in Table 5. Fig. 18 shows the comparisons between simulated and experimental forming results. It can be seen from Fig. 18(a) that the simulated thickness distribution along circumferential direction is very close to experimental result with the maximum relative error of 13.2%. As for the prediction accuracy of microstructure evolution, the microstructure at mid-thickness point was observed and compared with the simulated results, as shown in Fig. 18(b) and (c). The predicted and experimental DRX fractions are 0.612 and 0.581, respectively, presenting the relative error of 5.3%. As for β phase fractions, the predicted and experimental values are 0.228 and 0.212, respectively, with the relative error of 7.5%. Besides, the prediction of damage and fracture was also verified by a set of spinnability experiments. In spinnability experiments, the spinning thinning ratio increases gradually to produce fracture. In simulation, the void volume fraction (VVF) reaches the critical value of fracture when the thinning

ratio increases to 68.9%, as shown in Fig. 19(a). While, the fracture produces when the thinning ratio reaches 71.2% in experiment. The relative error of predicted limiting thinning ratio is 3.2%.

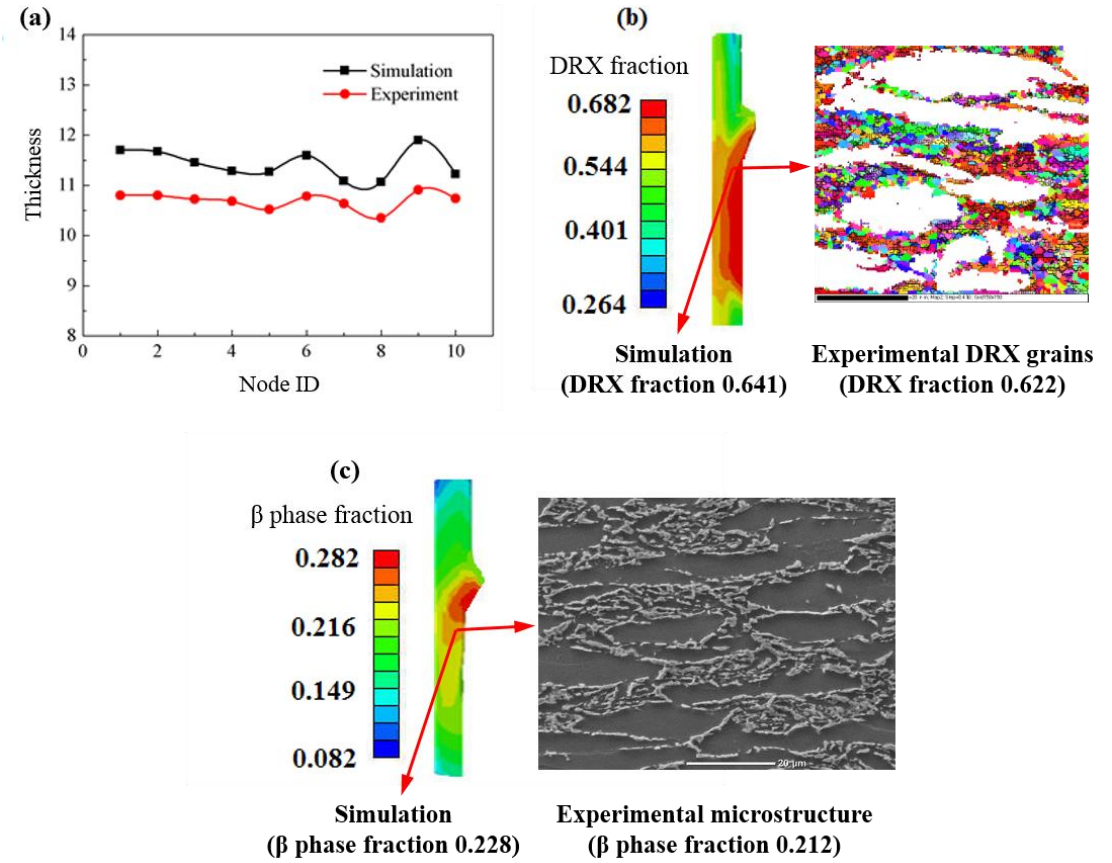

Fig. 18 Comparisons between the simulated and experimental results: (a) thickness distribution along circumferential direction; (b) DRX fraction; (c) β phase fraction.

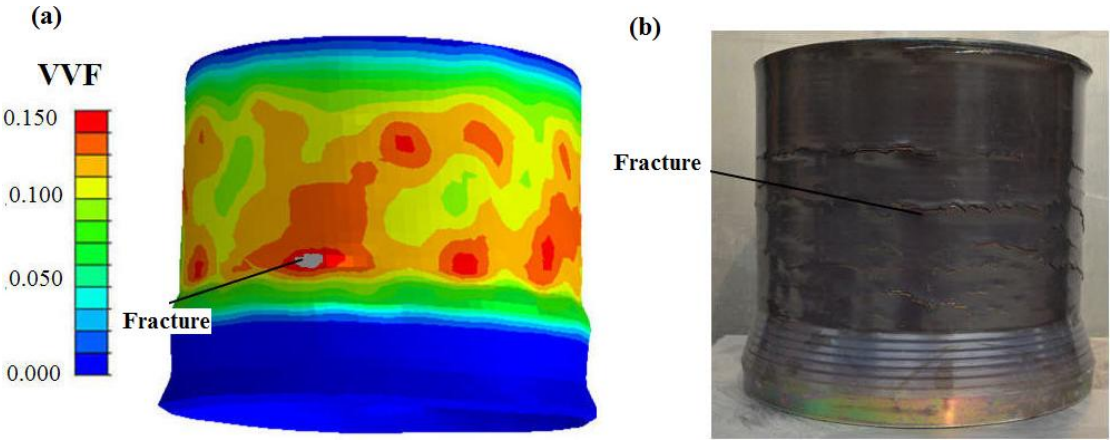

Fig. 19 Comparisons between the simulated damage and fracture at thinning ratio of 68.9% (a) and experimental fracture results at thinning ration of 71.2% (b).

The above comparisons suggest that the damage-coupled constitutive model proposed in this work is valid and can be applied in the FE modelling of hot working of TA15 alloy to predict the

macro-shape, DRX evolution, damage and fracture phenomena at the same time. It is helpful to reveal the microstructure evolution, damage and fracture behaviour of titanium alloy during hot deformation, and can provide important guidance for the coordinated control of microstructure and damage in the hot working of titanium alloy components.

6. Conclusions

In this paper, the microstructure, damage and flow behavior of TA15 alloy during hot tensile tests were experimentally analyzed. Based on the experimental results, a damage-coupled constitutive model considering microstructure evolution was developed. The following conclusions can be drawn:

(1) Increasing β phase fraction and DRX fraction would cause softening effect, relieve the local stress concentration, and thus supress the damage evolution (void nucleation, growth and coalescence). As a result, the fracture strain increases with both β phase fraction and DRX fraction in an exponential form. Besides, the stress state also presents great effect on the damage and fracture strain.

(2) A damage-coupled constitutive model considering microstructure evolution for hot deformation of titanium alloy was established. The model is mainly composed of three parts: microstructure model, damage model and constitutive law. The microstructure model considers the phase transformation, variation of dislocation density, DRX and loss of Hall-Petch strengthening, which is modelled using the internal variable method. The damage model considers the effects of microstructure and stress state on damage evolution, which is achieved by introducing β phase fraction, DRX fraction and stress triaxiality into the classical GTN model. The constitutive law considers both the effects of microstructure and damage evolution on flow behavior.

(3) The parameters in damage-coupled constitutive model were calibrated by comparing the predicted and experimental results. The developed model was successfully applied in the numerical simulation of hot spinning of TA15 alloy tube. It can accurately predict the macroscopic deformation, microstructure, damage and fracture during hot spinning, which verifies the reliability of constitutive model. The developed model can provide important guidance for the coordinated control of microstructure and damage in the hot working of titanium alloy components.

Acknowledgments

The authors would acknowledge the funding support from the National Science Fund for Distinguished Young Scholars of China (No. 51625505) and the Key Program Project of the Joint Fund of Astronomy and National Natural Science Foundation of China (No. U1537203), National Natural

Science Foundation of China (No. 51875467), the Hong Kong Scholar Program (No. XJ2018010) and the Young Elite Scientists Sponsorship Program by CAST (No. 2018QNRC001).

References

[1] D. Banerjee, J.C. Williams, Perspectives on Titanium Science and Technology, Acta Materialia 61(3) (2013) 844-879.

[2] G. Lütjering., J. C.Williams., <Titanium (2nd edition).pdf>, Springer-Verlag, Berlin Heidelberg (2007).

[3] P.F. Gao, Z.N. Lei, X.X. Wang, M. Zhan, Deformation in fatigue crack tip plastic zone and its role in crack propagation of titanium alloy with tri-modal microstructure, Materials Science and Engineering: A 739 (2019) 198-202.

[4] P.F. Gao, G. Qin, X.X. Wang, Y.X. Li, M. Zhan, G.J. Li, J.S. Li, Dependence of mechanical properties on the microstructural parameters of TA15 titanium alloy with tri-modal microstructure, Materials Science and Engineering: A 739 (2019) 203-213.

[5] J. Guo, M. Zhan, M.W. Fu, P.F. Gao, F. Ma, Extrapolation based constitutive modeling of flow stress of titanium alloy sheet under hot-working condition, Materials & Design 154 (2018) 96-107.

[6] S. Semiatin, V. Seetharaman, A. Ghosh, Plastic flow, microstructure evolution, and defect formation during primary hot working of titanium and titanium aluminide alloys with lamellar colony microstructures, Philosophical Transactions of the Royal Society of London. Series A: Mathematical, Physical and Engineering Sciences 357(1756) (1999) 1487-1512.

[7] S. Tamirisakandala, B.V. Vedam, R.B. Bhat, Recent Advances in the Deformation Processing of Titanium Alloys, Journal of Materials Engineering and Performance (2003).

[8] M. Zhan, T. Zhang, H. Yang, L. Li, Establishment of a thermal damage model for Ti-6Al-2Zr-1Mo-1V titanium alloy and its application in the tube rolling-spinning process, The International Journal of Advanced Manufacturing Technology 87(5-8) (2016) 1345-1357.

[9] X.G. Fan, H. Yang, P.F. Gao, Deformation behavior and microstructure evolution in multistage hot working of TA15 titanium alloy: on the role of recrystallization, Journal of Materials Science 46(18) (2011) 6018-6028.

[10] X.G. Fan, H. Yang, P.F. Gao, Prediction of constitutive behavior and microstructure evolution in hot deformation of TA15 titanium alloy, Materials & Design 51 (2013) 34-42.

[11] J. Luo, M. Li, X. Li, Y. Shi, Constitutive model for high temperature deformation of titanium alloys using internal state variables, Mechanics of Materials 42(2) (2010) 157-165.

[12] X.G. Fan, H. Yang, Internal-state-variable based self-consistent constitutive modeling for hot working of two-phase titanium alloys coupling microstructure evolution, International Journal of Plasticity 27(11) (2011) 1833-1852.

[13] P. Gao, H. Yang, X. Fan, S. Zhu, Unified modeling of flow softening and globularization for hot working of two-phase titanium alloy with a lamellar colony microstructure, Journal of Alloys and Compounds 600 (2014) 78-83.

[14] Q. Bai, J. Lin, T.A. Dean, D.S. Balint, T. Gao, Z. Zhang, Modelling of dominant softening mechanisms for Ti-6Al-4V in steady state hot forming conditions, Materials Science and Engineering: A 559 (2013) 352-358.

[15] B. Babu, L.-E. Lindgren, Dislocation density based model for plastic deformation and globularization of Ti-6Al-4V, International Journal of Plasticity 50 (2013) 94-108.

[16] G.R. Johnson, W.H. Cook, Fracture characteristics of three metals subjected to various strains, strain rates, temperatures and pressures, Engineering fracture mechanics 21(1) (1985) 31-48.

[17] J. He, Z. Cui, F. Chen, Y. Xiao, L. Ruan, The new ductile fracture criterion for 30Cr2Ni4MoV ultra-super-critical rotor steel at elevated temperatures, Materials & Design (1980-2015) 52 (2013) 547-555.

[18] B.T. Tang, S. Bruschi, A. Ghiotti, P.F. Bariani, An improved damage evolution model to predict fracture of steel sheet at elevated temperature, Journal of Materials Processing Technology 228 (2016) 76-87.

[19] L. Yang, B. Wang, G. Liu, H. Zhao, W. Xiao, Behavior and modeling of flow softening and ductile damage evolution in hot forming of TA15 alloy sheets, Materials & Design 85 (2015) 135-148.

[20] J. Li, B. Wang, H. Huang, S. Fang, P. Chen, J. Zhao, Y. Qin, Behaviour and constitutive modelling of ductile damage of Ti-6Al-1.5Cr-2.5Mo-0.5Fe-0.3Si alloy under hot tensile deformation, Journal of Alloys and Compounds 780 (2019) 284-292.

[21] J. Guo, M. Zhan, Y.Y. Wang, P.F. Gao, Unified modeling of work hardening and flow softening in two-phase titanium alloys considering microstructure evolution in thermomechanical processes, Journal of Alloys and Compounds 767 (2018) 34-45.

[22] K. Nahshon, J.W. Hutchinson, Modification of the Gurson Model for shear failure, European Journal of Mechanics - A/Solids 27(1) (2008) 1-17.

[23] L. Xue, Constitutive modeling of void shearing effect in ductile fracture of porous materials, Engineering Fracture Mechanics 75(11) (2008) 3343-3366.

[24] X. Shang, Z. Cui, M.W. Fu, Dynamic recrystallization based ductile fracture modeling in hot working of metallic materials, International Journal of Plasticity 95 (2017) 105-122.

[25] Z. Lei, P. Gao, H. Li, Y. Cai, M. Zhan, On the fracture behavior and toughness of TA15 titanium alloy with tri-modal microstructure, Materials Science and Engineering: A 753 (2019) 238-246.

[26] U.F. Kocks, H. Mecking, Physics and phenomenology of strain hardening: the FCC case, Progress in Materials Science 48(3) (2003) 171-273.

[27] S.L. Semiatin, T.R. Bieler, The effect of alpha platelet thickness on plastic flow during hot working of TI–6Al–4V with a transformed microstructure, Acta Materialia 49(17) (2001) 3565-3573.

[28] A.L. Gurson, Continuum Theory of Ductile Rupture by Void Nucleation and Growth: Part I—Yield Criteria and Flow Rules for Porous Ductile Media, Journal of Engineering Materials and Technology 99(1) (1977) 2-15.

[29] V. Tvergaard, A. Needleman, Analysis of the cup-cone fracture in a round tensile bar, Acta Metallurgica 32(1) (1984) 157-169.

[30] V. Tvergaard, Influence of voids on shear band instabilities under plane strain conditions, International Journal of Fracture 17(4) (1981) 389-407.

[31] V. Tvergaard, On localization in ductile materials containing spherical voids, International Journal of Fracture 18(4) (1982) 237-252.

[32] C.C. Chu, A. Needleman, Void Nucleation Effects in Biaxially Stretched Sheets, Journal of Engineering Materials and Technology 102(3) (1980) 249-256.